ADVANCES IN ATMOSPHERIC SCIENCES, VOL. 35, MAY 2018, 580–591

• **Original Paper** •

Characteristics and Preliminary Causes of Tropical Cyclone Extreme Rainfall Events over Hainan Island

Xianling JIANG[1,2,3,4], Fumin REN[*3], Yunjie LI[5], Wenyu QIU[6], Zhuguo MA[1], and Qinbo CAI[4]

[1]*Key Laboratory of Regional Climate–Environment for Temperate East Asia, Institute of Atmospheric Physics, Chinese Academy of Sciences, Beijing* 100029*, China*

[2]*University of Chinese Academy of Sciences, Beijing* 100049*, China*

[3]*State Key Laboratory on Severe Weather, Chinese Academy of Meteorological Sciences, Beijing* 100081*, China*

[4]*Hainan Meteorological Observatory, Haikou* 570203*, China*

[5]*Zhuhai Meteorological Bureau, Zhuhai* 519000*, China*

[6]*Key Laboratory of Meteorological Disaster of Ministry of Education, Nanjing University of Information Science and Technology, Nanjing* 210044*, China*

(Received 10 March 2017; revised 10 October 2017; accepted 24 October 2017)

ABSTRACT

The characteristics of tropical cyclone (TC) extreme rainfall events over Hainan Island from 1969 to 2014 are analyzed from the viewpoint of the TC maximum daily rainfall (TMDR) using daily station precipitation data from the Meteorological Information Center of the China Meteorological Administration, TC best-track data from the Shanghai Typhoon Institute, and NCEP/NCAR reanalysis data. The frequencies of the TMDR reaching 50, 100 and 250 mm show a decreasing trend [−0.7 (10 yr)$^{-1}$], a weak decreasing trend [−0.2 (10 yr)$^{-1}$] and a weak increasing trend [0.1 (10 yr)$^{-1}$], respectively. For seasonal variations, the TMDR of all intensity grades mainly occurs from July to October, with the frequencies of TMDR $\geqslant$ 50 mm and $\geqslant$ 100 mm peaking in September and the frequency of TMDR $\geqslant$ 250 mm [TC extreme rainstorm (TCER) events] peaking in August and September. The western region (Changjiang) of the Island is always the rainfall center, independent of the intensity or frequencies of different intensity grades. The causes of TCERs are also explored and the results show that topography plays a key role in the characteristics of the rainfall events. TCERs are easily induced on the windward slopes of Wuzhi Mountain, with the coordination of TC tracks and TC wind structure. A slower speed of movement, a stronger TC intensity and a farther westward track are all conducive to extreme rainfall events. A weaker northwestern Pacific subtropical high is likely to make the 500-hPa steering flow weaker and results in slower TC movement, whereas a stronger South China Sea summer monsoon can carry a higher moisture flux. These two environmental factors are both favorable for TCERs.

Key words: Hainan Island, tropical cyclones, extreme rainfall events, characteristics, causes

Citation: Jiang, X. L., F. M. Ren, Y. J. Li, W. Y. Qiu, Z. G. Ma, and Q. B. Cai, 2018: Characteristics and preliminary causes of tropical cyclone extreme rainfall events over Hainan Island. *Adv. Atmos. Sci.*, **35**(5), 580–591, https://doi.org/10.1007/s00376-017-7051-0.

1. Introduction

The influences of tropical cyclones (TCs) may vary regionally. TCs can bring abundant precipitation to dry regions, mitigating local droughts, but can also result in fierce winds and heavy precipitation, resulting in serious secondary disasters. Humans are more concerned about the latter effects, which pose a threat to both life and property. Many extreme rainfall events have been caused by TCs, with the potential risk of triggering floods, the overflow of rivers, and mudslides. It is therefore important to study the characteristics and mechanisms of extreme rainfall events caused by TCs.

Relevant studies have examined the temporal variations in extreme rainfall events caused by TCs. In China, the frequency of extreme rainfall events caused by TCs peaked in the 1970s and the number of stations observing these events reached its peak in the 1960s (Zhao and Wang, 2012). In southern China, more hourly extreme rainstorms induced by TCs occurred in the 1980s, while fewer occurred in the 1960s and the 1990s (Mao et al., 1996). TC extreme rainstorm (TCER) events (defined in section 2.2) occur every year in southern China, with an average, maximum, minimum and standard deviation of 15, 28, 5 and 6.7 yr^{-1}, respectively (Mao et al., 1996). TC-induced hourly extreme rainstorms occur from May to November in southern China, most frequently (30.7% of the total number of events) occurring in July (Mao et al., 1996).

* Corresponding author: Fumin REN
Email: fmren@163.com

A number of studies have shown that the triggering mechanisms of TC extreme rainfall events are not only determined by the characteristics of the TC, but are also governed by other factors, such as the topography, interactions between multi-scale circulation systems, and the formation and propagation of vortex Rossby waves and gravity inertia waves (Chen and Ding, 1979; Chen et al., 2002). Moisture convergence forced by high terrain has been shown to be an important factor in the enhancement of rainstorms (Powell, 1982; Lin et al., 2002; Chan and Liang, 2003; Duan and Chen, 2005; Duan et al., 2006; Gao et al., 2009; Tsai and Lee, 2009; Yang et al., 2011; Yu and Cheng, 2013; Yue et al., 2015). Planetary-scale systems, such as the ITCZ, the northwestern Pacific subtropical high (NWPSH), longwave troughs and ridges, and the jet stream, also provide favorable backgrounds for TC extreme rainfall events (Bosart and Lackmann, 1995; Qiu, 1997; Sun and Zhao, 2000; Zhang et al., 2001; Dong et al., 2006, 2010; Baek et al., 2013; Chen et al., 2014). Likewise, synoptic-scale and mesoscale systems enhance TC extreme rainfall events (Franklin et al., 2006; Atallah et al., 2007; Sawada and Iwasaki, 2010; Bao et al., 2015; Richard et al., 2015; Xu and Du, 2015). Some studies have shown that vortex Rossby waves and gravity inertia waves are active both before and during TC extreme rainfall events (Montgomery and Kallenbach, 1997; Chow et al., 2002; Yu, 2002). This suggests that many factors can cause TC extreme rainfall events, but that the causes may differ in different areas. Hainan Island is one of the most vulnerable places to be affected by TCs. Therefore, the specific factors that are important for Hainan Island deserve further research.

TC extreme rainfall events have been studied previously in the Hainan area. For example, Mao et al. (1996) reported that TCERs in Hainan tended to concentrate in the southwest quadrant of the typhoon. Both the frequency and accumulated amount of TC-induced extreme rainfall events have increased significantly in Hainan in the last 40 years (Wu et al., 2007). Cai et al. (2012) showed that the southwest monsoon and the terrain both contributed to the TC extreme rainfall events induced by typhoon Nesat in 2011. Other studies have also highlighted the important role of the topography of Hainan Island in inducing TC extreme rainfall events (Duan et al., 2006; Huang et al., 2010).

However, existing studies of TC extreme rainfall events have tended to focus on specific examples; the interannual variability and spatial distribution of TC extreme rainfall events in Hainan require further research. The similarities of weather conditions conducive to TC extreme rainfall events are worth studying. This paper reports the characteristics of TC extreme rainfall events on Hainan Island and considers the physical mechanisms underlying these events.

2. Data and methodology

2.1. *Data*

Daily precipitation data for Hainan Island are obtained from the Meteorological Information Center of the China Meteorological Administration for the period 1958–2014. A day is defined as 1200 UTC on the previous day to 1200 UTC on the same day. The best-track dataset for TCs in the Northwest Pacific (Ying et al., 2014) is provided by the Shanghai Typhoon Institute of the China Meteorological Administration. This dataset includes the positions and maximum winds near the centers of TCs at 6-h intervals from 1949 to 2014. NCEP reanalysis data ($2.5^\circ \times 2.5^\circ$ horizontal grid spacing; four times each day, including horizontal wind, specific humidity and geopotential height) from 1948 to 2014 (https://www.esrl.noaa.gov/psd/data/gridded/data.ncep.reanalysis.pressure.html) are adopted in this study. The percentage of days with missing data for all 18 stations is calculated. If this percentage exceeds 2.0% for a particular year, then the data for this year are ignored. The percentages are all $< 2.0\%$ after 1969, and therefore the period 1969–2014 is chosen as the study period.

Figure 1 shows how the elevation on Hainan Island increases gradually from the coast to the interior region. Wuzhi Mountain, with a height of 1867.1 m, is the highest point on the island. The local meteorological service divides Hainan Island into five subregions based on the topography and forecasting records: the northern region, the western region, the eastern region, the central region, and the southern region (Fig. 1). Haikou, Chengmai, Ding'an and Lin'gao stations are in the northern region; Danzhou, Baisha, Changjiang and Dongfang stations are in the western region; Wenchang, Qionghai and Wanning stations are in the eastern region; Tunchang, Qiongzhong and Wuzhishan stations are in the central region; and Sanya, Lingshui, Baoting and Ledong stations are in the southern region.

2.2. *Methodology*

An objective synoptic analysis technique, a dynamic composite analysis, and a TC track similarity method are applied in this study. The objective synoptic analysis technique, proposed by Ren et al. (2001, 2007, 2011), is utilized to partition the TC-induced rainfall from the total rainfall based on station observations.

Because TCs are moving systems, we perform a dynamic composite analysis (Gray, 1981; Li et al., 2004) that synthesizes atmospheric variables by tracing the centers of progressive TCs. This technique extracts the common features of circulation over the whole lifetime of the TC. The dynamic composite analysis is modified as follows: (a) extending the dynamic composite analysis to the environmental field; and (b) positioning the composite environmental field using the average position of the centers of the composited TCs.

The TC track similarity method (Ren et al., 2017) is conducted to objectively select TCs in similar tracks. Taking the area surrounded by any two tracks and the two line segments connecting the first two points and the last two points as the measuring criteria for similarity, this method gives full consideration to the position information of the whole lifetime of the TC.

This study focuses on the maximum amount of daily rainfall on Hainan Island caused by TCs, where each TC corre-

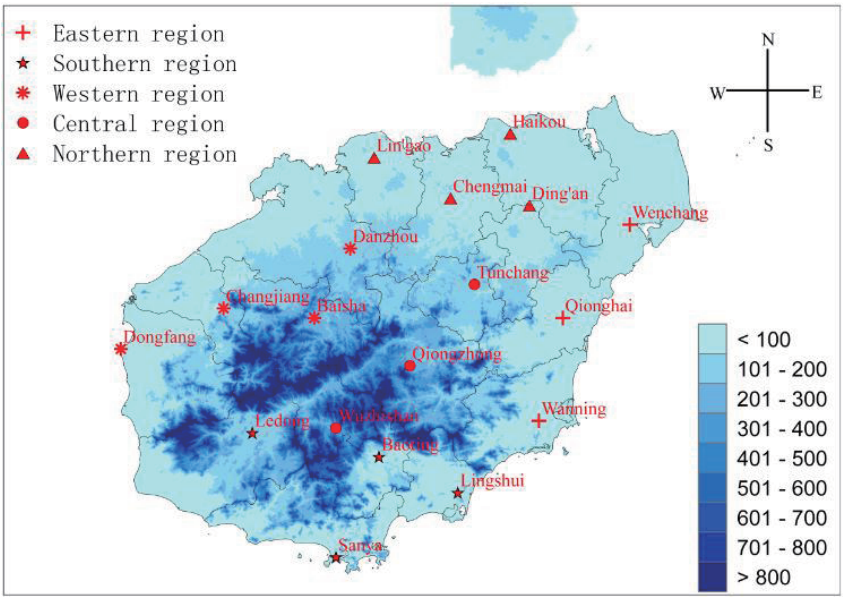

Fig. 1. Location of meteorological observation stations and topography (units: m) of Hainan Island.

sponds to one data point representing the TC maximum daily rainfall (TMDR), and pays particular attention to TC extreme rainstorm (TCER) events. The TC extreme rainfall events considered here include TC rainstorm events (100 mm > DR (daily rainfall) ⩾ 50 mm), TC heavy rainstorm events (250 mm > DR ⩾ 100 mm), and TCER events (DR ⩾ 250 mm).

3. Characteristics of TC extreme rainfall events

A total of 385 TCs affected Hainan Island from 1969 to 2014 (Fig. 2), defined as when precipitation caused by a TC is recorded by at least one of the 18 observation stations on Hainan Island. Among these 385 TCs, the rainfall of 113 (29.4%) TCs is below that of a rainstorm (50 mm). Eighty-eight (22.9%) and 145 (37.7%) TCs cause rainstorms and heavy rainstorms, respectively. The remaining 39 (10.1%) TCs create extreme rainstorms. The total percentages for all kinds of rainfall are > 100% due to rounding. Heavy rainstorms contribute the largest percentage value.

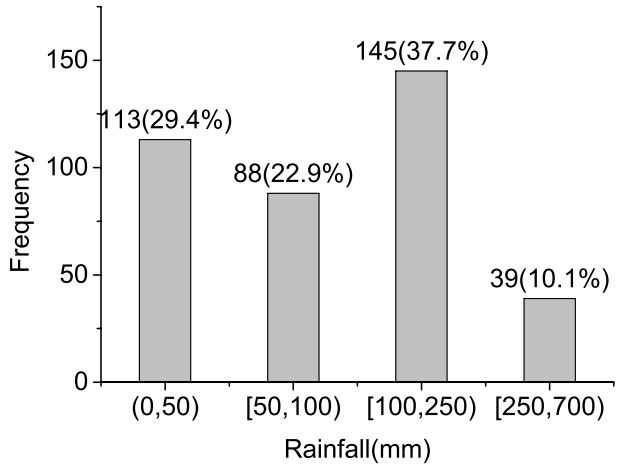

Fig. 2. Grade-frequency distribution of TMDR events over Hainan Island from 1969 to 2014.

Figure 3 shows the interannual and interdecadal variations in the TMDR in Hainan from 1969 to 2014. The frequency of the TMDR reaching 50 mm decreases at a rate of 0.7 (10 yr)$^{-1}$ at the 0.01 significance level (Fig. 3a). The nine-point moving average shows a quasi-20-year oscillation, with decreasing tendencies in the 1970s and 1990s and increasing tendencies in the 1980s and 2000s. The occurrence of TMDR reaching 100 mm shows a weaker decreasing trend of 0.3 (10 yr)$^{-1}$, which is not statistically significant. By contrast, the frequency of the TMDR reaching 250 mm shows a weak positive trend [0.1 (10 yr)$^{-1}$], which is not statistically significant. Figure 3c shows that more extreme rainstorms (DR ⩾ 250 mm) occurred during the most recent 10 years. This analysis illustrates that rainfall achieving the level of rainstorm (DR ⩾ 50 mm) has decreased in the past 46 years, whereas extreme rainstorms (DR ⩾ 250 mm) have increased, especially after 2004.

The frequency of TMDR ⩾ 50 mm over Hainan shows obvious seasonal characteristics (Fig. 4). TMDR ⩾ 50 mm may occur from April to December, but is mostly concentrated in July–October (79.8%) because typhoons occur more frequently in this season, with a maximum in September (22.8%). TMDR ⩾ 100 mm mainly occurs from May to November and is also concentrated in July–October (82.6%), reaching a peak in September (24.5%). TMDR ⩾ 250 mm (TCERs) occurs in May and July–November, centered in July–October (92.3%), with the most frequent occurrence in August and September (25.6% in each of these two months). These results are different from the analysis of Mao et al. (1996). It is possible that TCERs are showing a recent

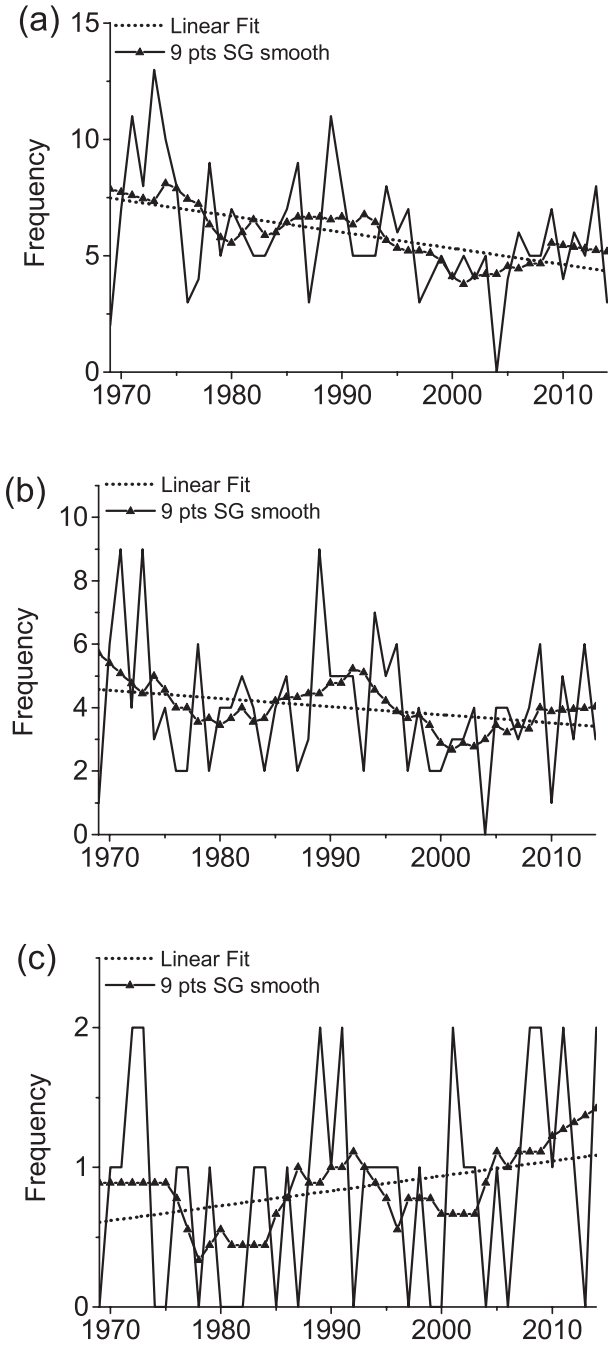

Fig. 3. Variations with time of TMDR statistics over Hainan Island from 1969 to 2014. Frequencies of daily rainfall of (a) $\geqslant 50$, (b) $\geqslant 100$ and (c) $\geqslant 250$ mm.

tendency to shift into autumn, or the research data and time periods may be different. Further analysis is needed. Events with different intensity grades of TMDR are all concentrated in summer to autumn. The most common three months of TMDR $\geqslant 50$ mm and $\geqslant 100$ mm are July, August and September, with the maximum in September. TMDR $\geqslant 250$ mm is more frequent in August, September and October, with the highest frequency in August and September.

Figure 5 shows the spatial distribution of TMDR statistics over Hainan Island for the period 1969–2014. Figure 5a

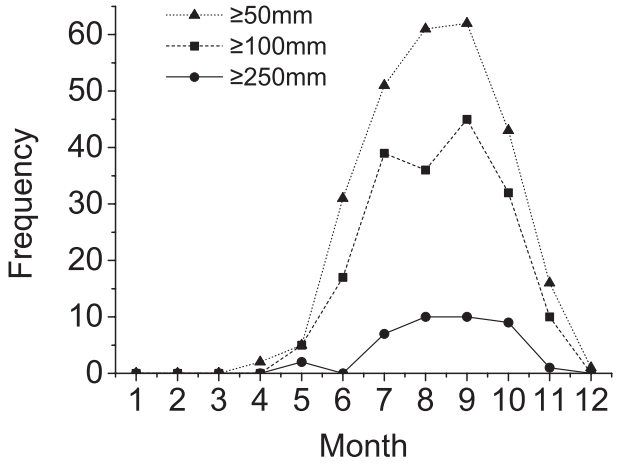

Fig. 4. Seasonal variations of TMDR statistics over Hainan Island from 1969 to 2014.

shows the distribution of the maximum TMDR of all 18 stations during the period 1969–2014. The recorded minimum is 210 mm and the maximum 644.6 mm, and each station reaches the TMDR during this period; the rainfall maxima are all > 100 mm. Rainfall > 450 mm occurs along the northern edge of Wuzhi Mountain from the western region to the eastern region, with the peak rainfall (644.6 mm) in the western region (Changjiang).

The frequency distributions of different grades of intensity (Figs. 5b–d) show that the western region (Changjiang) is always the rainfall frequency center for all intensities of rainfall, whereas the northern (Lin'gao) and central regions (Wuzhishan) are the secondary frequency centers for two (TMDR $\geqslant 50$ mm and TMDR $\geqslant 100$ mm) of the three grades of intensity.

Based on differences between areas, TCERs on Hainan Island can be divided into five distribution types. TMDR areas in the northern region, western region, eastern region, central region and southern region are called the northern region type, western region type, eastern region type, central region type and southern region type, respectively.

4. Effect of TC track and topography on TCER events

Figure 5 shows strong local features of TMDR maxima and frequencies of all rainfall intensity grades. In order to analyze its inducement, formation causes of TC extreme rainfall, especially TCERs, are explored. The causes of the formation of TCERs in each subregion of Fig. 1 are explored based on the TC track and the topography of Hainan Island. Then, the structures of TCs are studied by taking the western region type as a case study, because the TMDR of this type is more typical and stronger.

The results show that, for the five rainfall types (Fig. 6), the corresponding TCs mostly move to the west-northwest or northwest on or near Hainan Island on days with extreme rainstorms, although each rainfall type has its own charac-

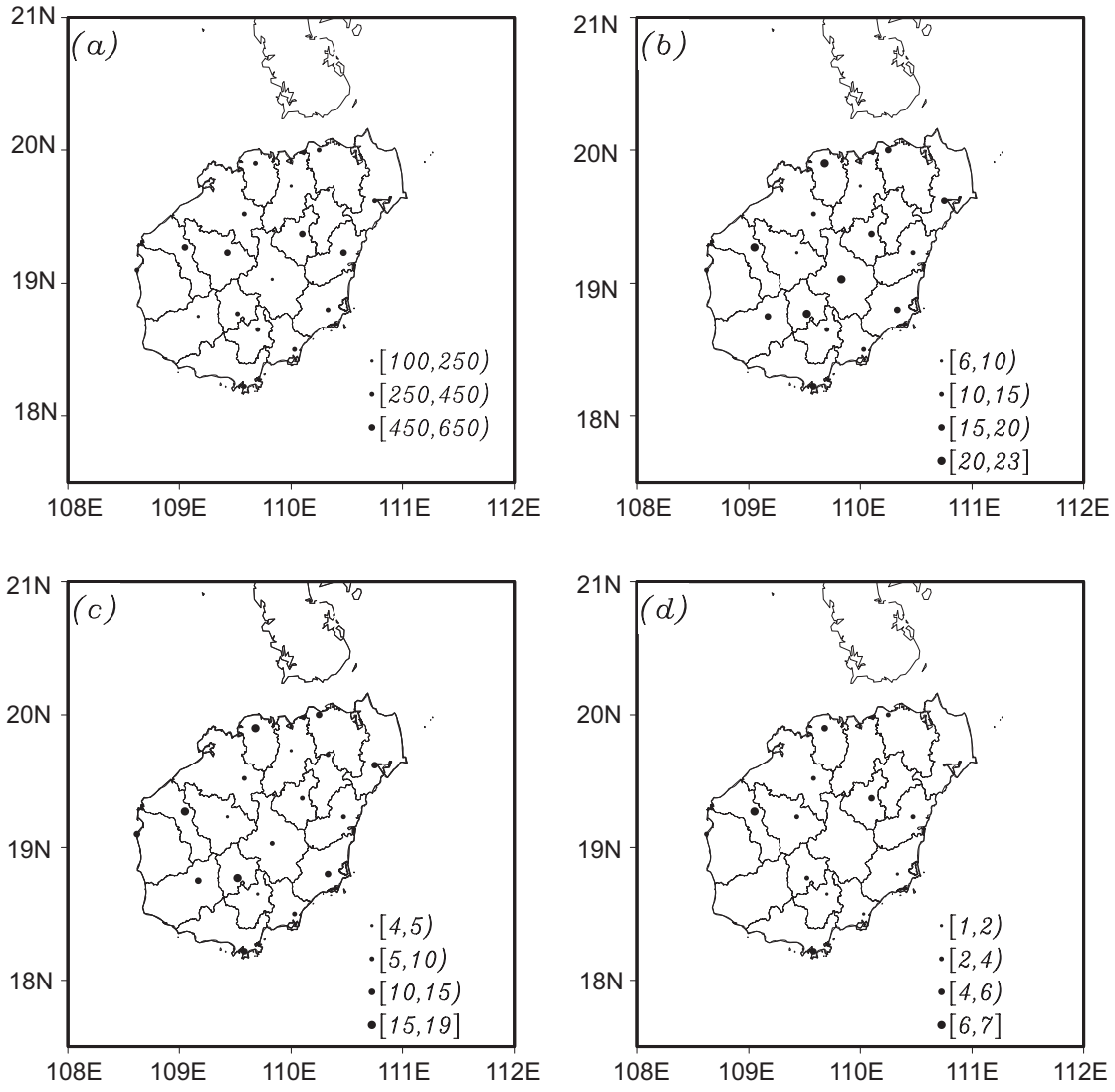

Fig. 5. Geographical distribution of TMDR statistics over Hainan Island from 1969 to 2014. (a) Maximum rainfall (units: mm), and frequency of daily rainfall of (b) ⩾ 50, (c) ⩾ 100 and (d) ⩾ 250 mm.

teristics. The western region type of TMDR has the highest number (14) of TCs, followed by the northern region type (eight TCs) and central region type (seven TCs). The numbers of southern region (six TCs) and eastern region (four TCs) types are lower. The TCs causing northern region–type TCERs move west-northwest, mostly making landfall north of Wuzhi Mountain and only once making landfall on the southern coast. These TCs, with only one exception, travel over Hainan Island on the north side of Wuzhi Mountain. The average path begins over the sea east of Hainan Island (112.6°E), passes through northern Wenchang to northeastern Haikou, Qiongzhou Strait and the southwestern Leizhou Peninsula, before reaching Beibu Gulf (109.3°E). The average horizontal wind over Hainan Island at 850 hPa is northerly (not shown) for the northern region–type TMDR events. Thus, the northern region is on the onshore side of the average TC track, which could enhance precipitation in the northern region as a result of frictional convergence. The northern region is also in close proximity to the average TC track and is therefore affected by the eyewall, which is often associated with heavy rainfall. Therefore, the position of the northern region may explain why the TMDR is high here.

The TC tracks of the western region type are more concentrated and make landfall along the band between the north of Wuzhi Mountain and the Leizhou Peninsula. They also move west-northwest, but their western components are more obvious. The TC tracks of the western region type TCs over the island are also to the north of Wuzhi Mountain, except for one TC. Compared with the average track of the northern region type, that of the western region type has a larger western component and a position farther west, beginning in the sea to the east of Hainan Island (111.4°E), moving through north-central Wenchang, northern Haikou, Qiongzhou Strait, and reaching the Beibu Gulf (107.8° E). The average horizontal wind of the western region type over Hainan Island at 850 hPa is northwesterly (not shown). Therefore, the western

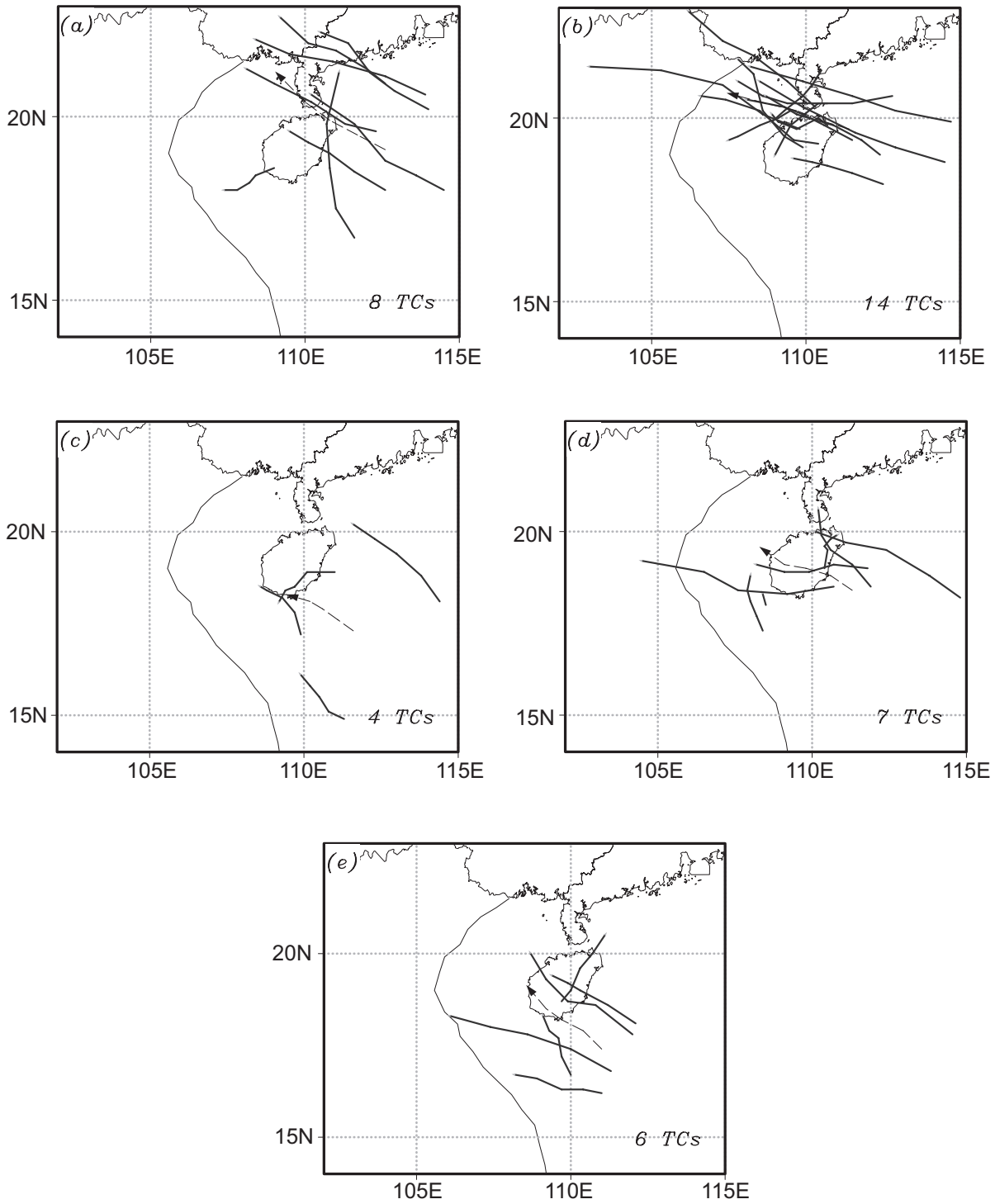

Fig. 6. TC tracks of different rainfall types on extreme rainstorm days over Hainan Island during 1969–2014 (arrows indicate the direction of movement of TCs and thick dashed lines represent the average TC tracks): (a) northern region type; (b) western region type; (c) eastern region type; (d) central region type; (e) southern region type.

region locates on the onshore side of the average TC track, which could enhance precipitation in the western region as a result of frictional convergence. The western region is located on the windward slope of Wuzhi Mountain in this case, which may enhance rainfall in the western region via friction and blocking effects.

The TC tracks of the eastern region type have no significant regularity and they are farther to the east and south. The tracks over the island pass through the southern half of Hainan Island. The average horizontal wind of the eastern region–type TCs over Hainan Island at 850 hPa is northeasterly (not shown). Therefore, the eastern region is also on the

onshore side or on the windward slope of Wuzhi Mountain.

The directions of movement of the central region–type TCs are consistent and are mostly west-northwest. Tracks over the island are evenly distributed in the different subregions and the average TC track passes through the central mountain subregion.

The TC tracks of the southern region type are relatively farther south and are scattered. The average TC track passes through the southern region, which means that most of the southern region is in close proximity to the onshore side of Wuzhi Mountain or on the windward slope of the mountain.

Thus, the different positions of TC tracks relative to Wuzhi Mountain can result in different areas of TCERs. Strong rainfall areas often occur in closer proximity to TCs, on the onshore flow sides of TCs, or on the windward slopes of Wuzhi Mountain, which is consistent with the results of Duan et al. (2006) and Huang et al. (2010).

Figure 5 shows that, over the 46-year period, the extreme values and frequencies of all grades of intensity of TMDR are highest in western Changjiang, which varies a lot from the adjacent stations. However, the distances from Changjiang to the TC centers do not favor the induction of strong rainfall (Fig. 7). The TCs with TMDR centers being in the western region of Hainan Island are in close proximity to the northern region of Hainan Island, or even pass through the northern region of Hainan Island, although the distances from Changjiang to the tracks of these TCs are greater. Therefore, strong rainfall in Changjiang may be closely associated with the terrain because rainfall on the windward slopes is often very different from that on the leeward slopes. Changjiang is located on the northwestern slope of Wuzhi Mountain in a gap between two mountains running east–west (Fig. 1). Changjiang is usually to the northwest or southwest of TCs, so the horizontal wind at low levels in Changjiang is either northwesterly or southwesterly (Fig. 7), placing Changjiang on the windward slope. Therefore, Changjiang is not only affected by wind funneling, but also by the uplifting and blocking effects of the two mountains.

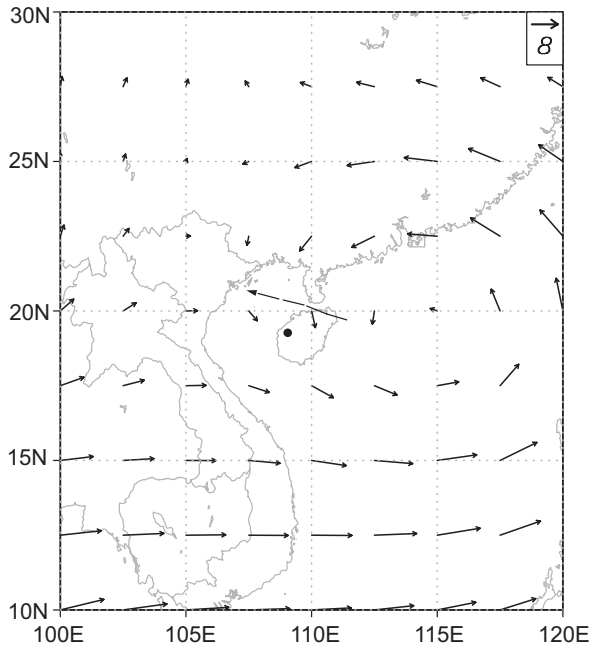

Fig. 7. Average TC track (thick dashed line with arrow) and composite horizontal wind field at 850 hPa (vectors; units: m s^{-1}) on extreme rainstorm days for western region–type TCs (black dot represents the position of Changjiang station).

The topography of the island (Elsberry, 1994) may also affect the distribution of heavy rainfall caused by TCs. When a TC approaches one side of a large island, an induced vortex may be generated on the other side of the island because of the local strengthening of the relative positive vorticity on the leeward side of the island or the forcing effect on the local circulation at low levels by the island topography. Under appropriate conditions, the center of the TC at high levels could couple with this induced vortex. A sudden heavy rainfall event might occur where the vortex is generated. Figure 6b shows that most TCs make landfall in the east of Hainan Island and Changjiang is located in the west of the island, which may well be in agreement with these results. The heavy rainfall in Changjiang is probably thus closely related to the terrain, the TC track, and the wind structure of the TC.

5. Effect of the characteristics of TCs and the environment on TCER events

The tracks of the western region–type rainfall events are more consistent and do not diverge as much as the other types of rainfall events; as such, they have an increased regularity. Therefore, the western region type is selected to explore the effects of the characteristics of TCs and environmental factors on TCERs. Among the 385 TCs affecting Hainan Island from 1969 to 2014, there are 56 TCs whose TMDR centers are located in the western region and that induce rainfall $\geqslant 50$ mm. The TC track similarity method is used to select five strong rainfall TCs and five weak rainfall TCs from these 56 TCs for further analysis.

An appropriate TC is first chosen as the reference TC based on the TMDR amount. Because the TC associated with the largest TMDR is an isolated event, it is difficult and inappropriate to use it to calculate the TC similarity area index (TSAI). Therefore, we choose Typhoon Rammasun (2014), whose TMDR ranks second, as the reference TC. The TSAI between the reference TC and the other 55 TCs is then calculated and two groups of appropriate TCs are determined. Using the ranks of TSAI, four TCs with strong rainfall are selected with the reference TC as the strong rainfall TC group, and five TCs with weak rainfall as the weak rainfall TC group.

Table 1 compares the strong (weak) western region–type TCs. For strong-rainfall TCs, the daily rainfall maximum is 644.6 mm and the minimum is 356.0 mm; whereas, for weak-rainfall TCs, the maximum rainfall is 185.1 mm and the minimum is 104.0 mm. Considering that maximum daily rainfall may occur in June, July, August and September, and

Table 1. Comparison of the two groups of western region–type TCs on extreme rainfall days over Hainan Island.

	TC name (number)	TMDR (mm)	Month
Strong western region–type TCs	Fitow (0114)	644.6	August
	Rammasun (1409)	544.3	July
	Sarah (7703)	490.3	July
	Willie (9618)	423.1	September
	Kate (7311)	356.0	August
Weak western region–type TCs	Dinah (7406)	185.1	June
	S.T.S. (8011)	172.5	August
	Jebi (1309)	167.8	August
	Faye (8907)	163.4	July
	Nina (9511)	104.0	September

the frequencies are fairly even, we can exclude the impact of seasonal variations. The TC tracks of the two groups are similar and both move west-northwest or west through the band from northern Hainan Island to Leizhou Peninsula, reaching Beibu Gulf, with several TCs making landfall again (not shown). The distinction between the two groups is that TCs with strong rainfall move along a track that is farther south and with slower speed, and then a shorter track (Fig. 8a).

Sometimes, the individual characteristics of TCs may have important functions in the formation of TCER events. Figure 8b presents the average values of the TMDR, maximum wind speed, TC moving speed, and direction deviation index, for the two groups of strong and weak TCs. The direction deviation index of a TC is the counterclockwise rotation angle from due west to the direction of movement in units of degrees (°). For example, when a TC travels due west, its direction deviation index is 0°, whereas when a TC travels northwest its direction deviation index is 315°. Figure 8 shows that the TMDR of the two groups varies widely, with differences > 300 mm, passing the statistical test at a significance level of 0.001.

The average maximum wind speed of strong-rainfall TCs is greater than that of weak-rainfall TCs, with the difference reaching 6.64 m s^{-1}, which is not statistically significant. The average moving speed of strong-rainfall TCs is significantly slower than that of weak-rainfall TCs, with an absolute difference of 9.08 km h^{-1} and relative difference of 61.5%, which is statistically significant at a level of 0.01. Slower TC moving speeds favor maintaining precipitation at a certain place for a longer time, which is likely to cause TCER events. The average direction deviation index of the strong-rainfall TC group is larger than that of the weak-rainfall TC group, which means the westward-moving component of the strong-TC group is larger and the TC centers are closer to the western region (Fig. 8a) and are thus conducive to heavy precipitation in the western region. The intensity, speed and direction deviation index of the strong-rainfall TC group are therefore all conducive to heavy or extreme rainfall events.

This analysis detects significant differences between the characteristics of TCs in the two groups. These differences are fundamentally related to the local environment, so deeper analysis of the similarities and differences in the local environment between the two groups is required.

One of the main conditions of inducing TCER events is a steady and continuous supply of moisture. For the dynamic composite moisture flux at 850 hPa (Figs. 9a and b), strong-rainfall TCs are related to a stronger moisture flux, which provides adequate moisture and leads to the lower atmosphere of the future torrential rain zone becoming wetter. This may accumulate large amounts of unstable energy and accelerate the convective instability of TCER events. There are three regions in which the central moisture flux is > 16 g s^{-1} Pa^{-1} m^{-1} as a result of mesoscale pulsations in wind speed. These pulsations are more important than the low-level jet itself. It has been observed that a rainstorm is often accompanied by several centers of maximum wind speed propagating downstream along the jet axis. For the weak rainfall TCs, the linked moisture flux values are relatively

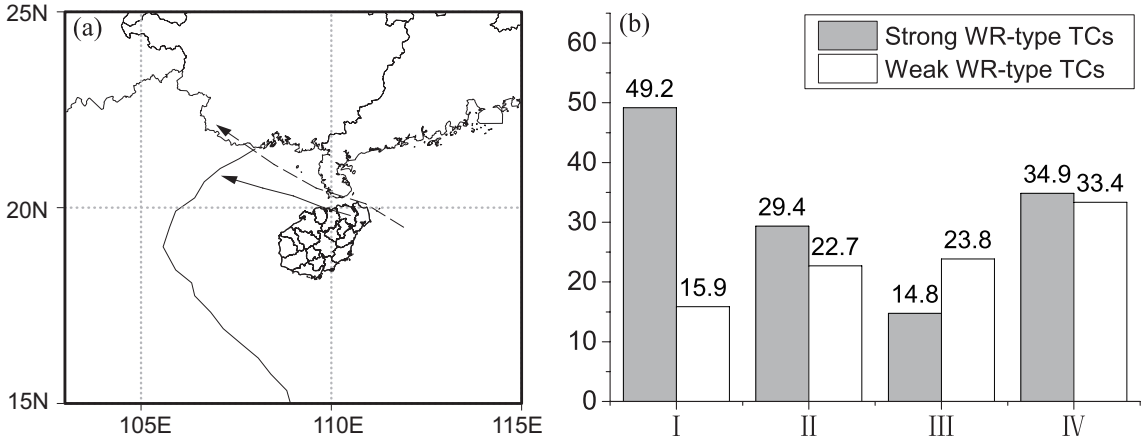

Fig. 8. (a) Average tracks and (b) characteristic statistics of the strong (weak) western region–type TC group on extreme rainfall days over Hainan Island. I, II, III and IV represent TMDR events (units: 10 mm), the maximum wind speed (units: m s^{-1}), the speed of movement (units: km h^{-1}) and the direction deviation index (units: 10°), respectively. The solid (dashed) line with arrow is the average track of strong (weak) western region–type TCs.

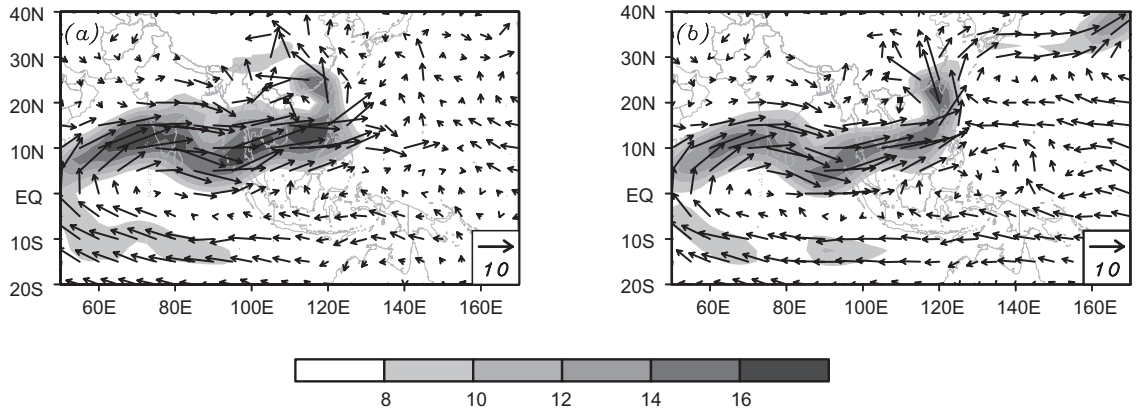

Fig. 9. Distribution of composite moisture fluxes (units: g s^{-1} Pa^{-1} m^{-1}; shaded areas indicate vector magnitude ⩾ 8 g s^{-1} Pa^{-1} m^{-1}) for the two western region–type TCs on extreme rainfall days at 850 hPa: (a) strong western region–type TCs; (b) weak western region–type TCs.

small; the area reaching 8 g s^{-1} Pa^{-1} m^{-1} is smaller and the values of very few regions are > 16 g s^{-1} Pa^{-1} m^{-1}. In the strong-rainfall TC group, the majority of water vapor is transported into the wind circulation, whereas a portion of the water vapor in the weak-rainfall TC group is transported to the distant ocean. All these conditions may result in stronger low-level moisture convergence and release more latent heat to maintain the warm-core structures of strong-rainfall TCs. The moisture flux divergence difference (not shown) at 850 hPa supports this. The moisture divergence of the strong-rainfall TC group is larger, with the center value reaching (9–12) $\times 10^{-6}$ g s^{-1} Pa^{-1} m^{-2}, whereas the weak-rainfall TC group only reaches (6–9) $\times 10^{-6}$ g s^{-1} Pa^{-1} m^{-2}. The difference between them is (4–6) $\times 10^{-6}$ g s^{-1} Pa^{-1} m^{-2}. A strong supply of moisture is therefore an important condition of TCER events.

TCER events accompany the intensification of the South China Sea summer monsoon (SCSSM) [defined as the 850-hPa mean zonal wind over (5–15°N, 105–120°E) of the southern South China Sea during a short period] (Fig. 10). Both strong- and weak-rainfall TCs have a monsoon surge before the TMDR event occurs. The SCSSM index generally begins to increase five days before the TMDR event day, increases quickly three to four days before the day of the TMDR event, and reaches the highest value one day before the TMDR event. After the day of the TMDR event, the SCSSM index reduces rapidly. The obvious difference between strong- and weak-rainfall TCs is the intensity of the SCSSM. During the period from seven days before to three days after the day of the TMDR event, the SCSSM index of strong rainfall TCs is always higher than that of the weak rainfall TC group. Therefore, the SCSSM has a close relationship with TMDR events and a strong SCSSM might induce TCER events.

Figure 11 shows the contrast in the circulation of the NWPSH at 500 hPa for the two groups of TCs. The area enclosed by the 5880-gpm line is smaller for strong-rainfall TCs, which means that the NWPSH is relatively weak. The zonal distance from the western ridge point to the center of

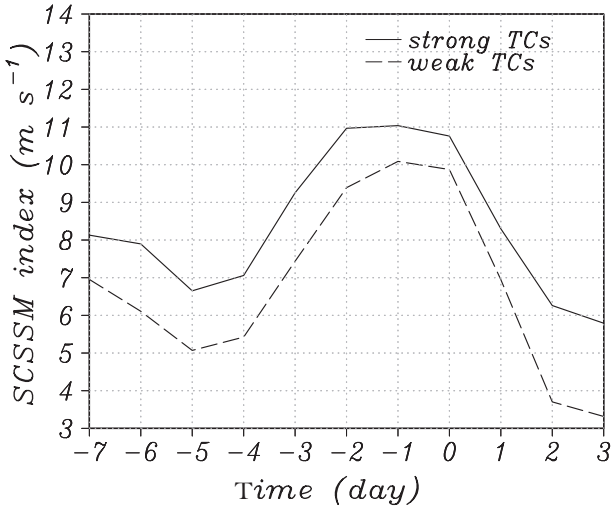

Fig. 10. Daily variation of the composite SCSSM index for the two western region–type TCs (on the abscissa, 0 represents the extreme rainfall day).

the TC is about 12° of longitude. The NWPSH is squeezed by the southwesterly jet and the TC circulation, which is not conducive to the steering role of the NWPSH on the TC track. The confrontation between the southwestly jet and the NWPSH tends to make TCs move slowly, which gives them more time to cause heavy rain on land. For weak-rainfall TCs, the NWPSH is stronger, the area surrounded by the 5880-gpm line is larger, and the zonal distance from the western ridge point to the center of the TC is only about 7° of longitude. In addition, the wind speed near the NWPSH is larger and the southeasterly wind southwest of the NWPSH makes the TC move faster, which reduces the likelihood of strong rainfall being maintained in a certain area.

The strong zone of westerly winds southwest of the strong-rainfall TC circulation has a broad range, which has the benefit of bringing in more moisture. A constant supply of moisture transported into the circulation of the TC results in warming, humidification and maintenance of the circula-

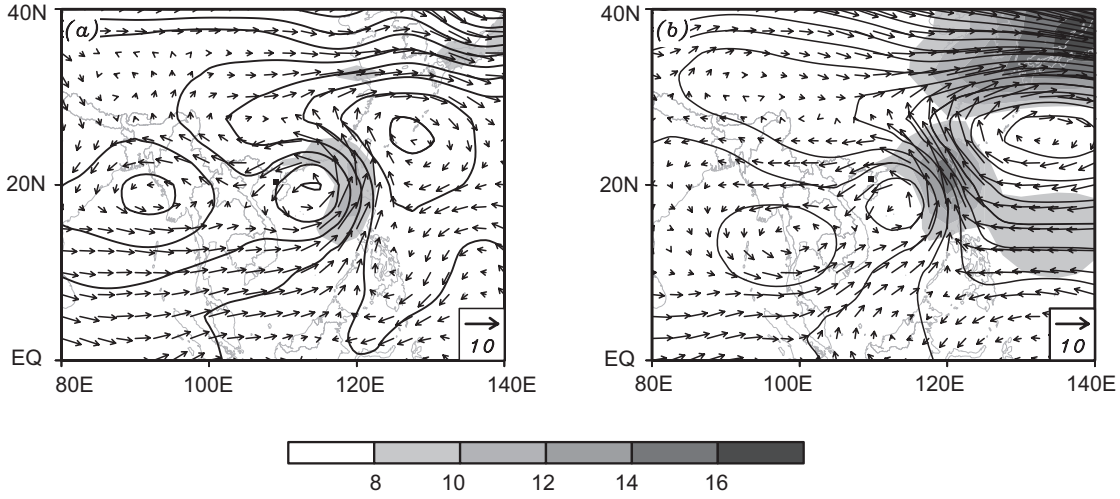

Fig. 11. Distribution of composite horizontal wind (vectors; units: m s^{-1}; shaded areas indicate wind vector magnitudes $\geqslant$ 8 m s^{-1}) and geopotential height (contours; units: gpm; thick solid lines represent the lines of 5880 gpm) fields for the two western region–type TCs on extreme rainfall days at 500 hPa: (a) strong western region–type TCs; (b) weak western region–type TCs.

tion of the TC. The strong westerly wind zone of the circulation of weak-rainfall TCs is smaller and brings less moisture into the circulation of the TC. In addition, some of the moisture is transported to the distant sea by the NWPSH, which is not conducive to developing strong rainfall events.

No significant difference is found between the two groups of TCs in the geopotential height field at 100 hPa and wind divergence at 200 hPa (not shown), indicating that high-level circulation has little effect on the difference in rainfall between the two types of TC.

6. Summary and discussion

Characteristics of extreme rainfall events over Hainan Island and their causes are investigated from 1969 to 2014 using NCEP/NCAR reanalysis data, station precipitation data, and TC best-track data. The main results are as follows:

(1) During the period 1969–2014, the frequencies of TMDR events reaching 50, 100 and 250 mm show a significantly decreasing trend [−0.7 (10 yr)$^{-1}$], a weakly decreasing trend [−0.2 (10 yr)$^{-1}$] and a weakly increasing trend [0.1 (10 yr)$^{-1}$], respectively.

(2) In terms of seasonal variations, TMDR events of all intensity grades occur mainly in July to October, with the frequencies of TMDR events $\geqslant$ 50 mm and $\geqslant$ 100 mm peaking in September, whereas the frequency of TMDR events $\geqslant$ 250 mm peak in August and September.

(3) In terms of geographical distribution, TMDR events can occur anywhere over Hainan Island with daily rainfall maxima > 100 mm. The western region (Changjiang) is always the rainfall center, independent of the intensity or frequencies of different grades of intensity. The maximum daily rainfall at Changjiang is 644.6 mm and the frequencies of events with TMDR $\geqslant$ 50 mm, $\geqslant$ 100 mm and $\geqslant$ 250 mm are 23, 19 and 7, respectively.

(4) Topography plays a key role in the geographical distribution of TMDR events. With the coordination of the track and wind structure of TCs, TCER events are easily induced on the windward slopes of Wuzhi Mountain, especially in the western region of Changjiang.

(5) Comparison of the strong (weak) western region–type TCs shows differences in the characteristics and environments of TCs. A slower moving speed, a stronger TC intensity and a track that is farther west are all conducive to heavy or extreme rainfall events. In terms of the role of the environment, a weaker NWPSH is likely to make the 500-hPa steering flow weaker and results in slower movement of the TC, whereas a stronger SCSSM can carry a higher moisture flux. These two environmental factors both favor extreme rainstorms.

This study has resulted in some meaningful conclusions on TMDR events, based on which the centers of rainfall can be determined more accurately and quickly when a TC moves over or near Hainan Island. However, there are still some problems and deficiencies that require further analysis. For instance, this paper focuses on diagnostic analysis, but the physical mechanisms of some of the conclusions (such as the role of Wuzhi Mountain) need to be verified through numerical simulations, which will be carried out in future research.

Acknowledgements. This research was jointly supported by the National Natural Science Foundation of China (Grant No. 41375056), the National Science-Technology Support Plan Project (Grant No. 2013BAK05B03), the Hainan Meteorological Service Research Project (Grant No. HNQXQN201402), the China Meteorological Administration Forecaster Special Project (Grant No. CMAYBY2015-058) and the National Natural Science Foundation of China (Grant No. 41675042).

REFERENCES

Atallah, E., L. F. Bosart, and A. R. Aiyyer, 2007: Precipitation distribution associated with landingfalling tropical cyclones over the eastern United States. *Mon. Wea. Rev.*, **135**, 2185–2206, https://doi.org/10.1175/MWR3382.1.

Baek, E.-H., J.-H. Kim, J.-S. Kug, G.-H. Lim, 2013: Favorable versus unfavorable synoptic backgrounds for indirect precipitation events ahead of tropical cyclones approaching the Korean Peninsula: A comparison of two cases. *Asia-Pacific Journal of Atmospheric Sciences*, **49**, 333–346, https://doi.org/10.1007/s13143-013-0032-z.

Bao, X. W., and Coauthors, 2015: Diagnostics for an extreme rain event near Shanghai during the Landfall of Typhoon Fitow (2013). *Mon. Wea. Rev.*, **143**, 3377–3405, https://doi.org/10.1175/MWR-D-14-00241.1.

Bosart, L. F., and G. M. Lackmann, 1995: Postlandfall tropical cyclone reintensification in a weakly baroclinic environment: A case study of hurricane david (September 1979). *Mon. Wea. Rev.*, **123**, 3268–3291, https://doi.org/10.1175/1520-0493(1995)123<3268:PTCRIA>2.0.CO;2.

Cai, X. H., R. Y. Yang, G. H. Zhou, and Z. H. Guo, 2012: Analysis on heavy rainfall process caused by 1117 strong typhoon " Neuchatel " in Hainan Island. *Journal of Meteorological Research and Application*, **33**, 5–8, https://doi.org/10.3969/j.issn.1673-8411.2012.02.002. (in Chinese with English abstract)

Chan, J. C. L., and X. D. Liang, 2003: Convective asymmetries associated with tropical cyclone landfall. Part I: *F*-plane simulations. *J. Atmos. Sci.*, **60**, 1560–1576, https://doi.org/10.1175/1520-0469(2003)60<1560:CAAWTC>2.0.CO;2.

Chen, B.-F., R. L. Elsberry, and C.-S. Lee, 2014: Origin and maintenance of the long-lasting, outer mesoscale convective system in typhoon Fengshen (2008). *Mon. Wea. Rev.*, **142**, 2838–2859, https://doi.org/10.1175/MWR-D-14-00036.1.

Chen, L. S., and Y. H. Ding, 1979: *An Introduction to the West Pacific Typhoons*. Science Press, 440–488. (in Chinese)

Chen, L. S., X. D. Xu, Z. X. Luo, and J. Z. Wang, 2002: *Introduction to Tropical Cyclone Dynamics*. China Meteorological Press, 317 pp. (in Chinese)

Chow, K. C., K. L. Chan, and A. K. H. Lau, 2002: Generation of moving spiral bands in tropical cyclones. *J. Atmos. Sci.*, **59**, 2930–2950, https://doi.org/10.1175/1520-0469(2002)059<2930:GOMSBI>2.0.CO;2.

Dong, M. Y., G. Y. Xue, and P. Q. Zheng, 2006: Study on the characteristics of tropical cyclones activity over the western North Pacific in 2004 and the cause of formation. *Journal of Tropical Meteorology*, **22**, 498–504, https://doi.org/10.3969/j.issn.1004-4965.2006.05.013. (in Chinese with English abstract)

Dong, M. Y., L. S. Chen, Y. Li, and C. G. Lu, 2010: Rainfall reinforcement associated with landfalling tropical cyclones. *J. Atmos. Sci.*, **67**, 3541–3558, https://doi.org/10.1175/2010JAS3268.1.

Duan, L., and L. S. Chen, 2005: Diagnostic analysis and numerical study of torrential rain associated with the tropical storm Fitow (0114). *Chinese Journal of Atmospheric Sciences*, **29**, 343–353, https://doi.org/10.3878/j.issn.1006-9895.2005.03.02. (in Chinese with English abstract)

Duan, L., L. S. Chen, and X. D. Xu, 2006: The numerical simulation on the impact of topography on the structure change and motion of tropical storm Fitow (0114). *Acta Meteorologica Sinica*, **64**, 186–193, 258, https://doi.org/10.3321/j.issn:0577-6619.2006.02.006. (in Chinese)

Elsberry, R. L., 1994: *A Global View of Tropical Cyclones*. L. S. Chen, Trans., China Meteorological Press, 341 pp. (in Chinese)

Franklin, C. N., G. J. Holland, and P. T. May, 2006: Mechanisms for the generation of mesoscale vorticity features in tropical cyclone rainbands. *Mon. Wea. Rev.*, **134**, 2649–2669, https://doi.org/10.1175/MWR3222.1.

Gao, S. Z., Z. Y. Meng, F. Q. Zhang, and L. F. Bosart, 2009: Observational analysis of heavy rainfall mechanisms associated with severe tropical storm Bilis (2006) after its landfall. *Mon. Wea. Rev.*, **137**, 1881–1897, https://doi.org/10.1175/2008MWR2669.1.

Gray, W. M., 1981: Recent advances in tropical cyclone research from rawinsonde composite analysis. WMO Program on Research in Tropical Meteorology. Fort Collins, Colorado, 407 pp.

Huang, P., H. P. Huang, H. J. Chen, and Y. Zheng, 2010: Analysis on moving path of tropical storm "SWAN" (No. 0907) and its torrential rain. *Journal of Meteorological Research and Application*, **31**, 5–8, https://doi.org/10.3969/j.issn.1673-8411.2010.03.002. (in Chinese with English abstract)

Li, Y., L. S. Chen, and J. Z. Wang, 2004: The diagnostic analysis on the characteristics of large scale circulation corresponding to the sustaining and decaying of tropical cyclone after it's landfall. *Acta Meteorologica Sinica*, **62**, 167–179, https://doi.org/10.3321/j.issn:0577-6619.2004.02.004. (in Chinese with English abstract)

Lin, Y.-L., D. B. Ensley, S. Chiao, and C.-Y. Huang, 2002: Orographic influences on rainfall and track deflection associated with the passage of a tropical cyclone. *Mon. Wea. Rev.*, **130**, 2929–2950, https://doi.org/10.1175/1520-0493(2002)130<2929:OIORAT>2.0.CO;2.

Mao, X., Z. He, and S. R. Mao, 1996: Statistical features of unusually heavy rainstorms by tropical cyclones in southern China. *Journal of Tropical Meteorology*, **12**, 78–84, https://doi.org/10.16032/j.issn.1004-4965.1996.01.011. (in Chinese with English abstract)

Montgomery, M. T., and R. J. Kallenbach, 1997: A theory for vortex rossby-waves and its application to spiral bands and intensity changes in hurricanes. *Quart. J. Roy. Meteor. Soc.*, **123**, 435–465, https://doi.org/10.1002/qj.49712353810.

Powell, M. D., 1982: The transition of the hurricane Frederic boundary-layer wind field from the open gulf of Mexico to landfall. *Mon. Wea. Rev.*, **110**, 1912–1932, https://doi.org/10.1175/1520-0493(1982)110<1912:TTOTHF>2.0.CO;2.

Qiu, Y. Y., 1997: Weather patterns and interannual variations of typhoon torrential rain during midsummer in North China. *Meteorological Monthly*, **23**, 3–9. (in Chinese with English abstract)

Ren, F. M., B. Gleason, and D. R. Easterling, 2001: A numerical technique for partitioning cyclone tropical precipitation. *Journal of Tropical Meteorology*, **17**, 308–313, https://doi.org/10.3969/j.issn.1004-4965.2001.03.015. (in Chinese with English abstract)

Ren, F. M., Y. M. Wang, X. L. Wang, and W. J. Li, 2007: Estimating tropical cyclone precipitation from station observations. *Adv. Atmos. Sci.*, **24**, 700–711, https://doi.org/10.1007/s00376-007-0700-y.

Ren, F. M., G. X. Wu, X. L. Wang, Y. M. Wang, W. J. Dong, J. Liang, and L. N. Bai, 2011: *Tropical Cyclones Affecting China Over the Last* 60 *Years*. China Meteorological Press,

203 pp. (in Chinese)

Ren, F. M., W. Y. Qiu, C. C. Ding, X. L. Jiang, L. G. Wu, Y. L. Xu, and Y. H. Duan, 2017: An Objective Index of Tropical Cyclone Track Similarity and Its Preliminary Application in the Prediction of the Precipitation Associated with Landfalling Tropical Cyclones. *Quart. J. Roy. Meteor. Soc.*, submitted.

Richard, C. Y. L., W. Zhou, and T. C. Lee, 2015: Climatological characteristics and observed trends of tropical cyclone-induced rainfall and their influences on long-term rainfall variations in Hong Kong. *Mon. Wea. Rev.*, **143**, 2192–2206, https://doi.org/10.1175/MWR-D-14-00332.1.

Sawada, M., and T. Iwasaki, 2010: Impacts of evaporation from raindrops on tropical cyclones. Part II: Features of rainbands and asymmetric structure. *J. Atmos. Sci.*, **67**, 84–96, https://doi.org/10.1175/2009JAS3195.1.

Sun, J. H., and S. X. Zhao, 2000: Diagnoses and simulations of typhoon (Tim) landing and producing heavy rainfall in China. *Chinese Journal of Atmospheric Sciences*, **24**, 223–237, https://doi.org/10.3878/j.issn.1006-9895.2000.02.11. (in Chinese)

Tsai, H.-C., and T. H. Lee, 2009: Maximum covariance analysis of typhoon surface wind and rainfall relationships in Taiwan. *Journal of Applied Meteorology and Climatology*, **48**, 997–1016, https://doi.org/10.1175/2008JAMC1963.1.

Wu, Y. J., S. A. Wu, and P. M. Zhai, 2007: The impact of tropical cyclones on Hainan island's extreme and total precipitation. *International Journal of Climatology*, **27**, 1059–1064, https://doi.org/10.1002/joc.1464.

Xu, H. X., and B. Du, 2015: The impact of typhoon Danas (2013) on the torrential rainfall associated with typhoon Fitow (2013) in East China. *Advances in Meteorology*, **2015**, 383712, https://doi.org/10.1155/2015/383712.

Yang, M.-J., S. A. Braun, and D.-S. Chen, 2011: Water budget of typhoon Nari (2001). *Mon. Wea. Rev.*, **139**, 3809–3828, https://doi.org/10.1175/MWR-D-10-05090.1.

Ying, M., W. Zhang, H. Yu, X. Lu, J. Feng, Y. Fan, Y. Zhu, and D. Chen, 2014: An overview of the China Meteorological Administration tropical cyclone database. J. Atmos. Oceanic Technol., 31, 287–301, https://doi.org/10.1175/JTECH-D-12-00119.1.

Yu, C.-K., and L.-W. Cheng, 2013: Distribution and mechanisms of orographic precipitation associated with typhoon Morakot (2009). *J. Atmos. Sci.*, **70**, 2894–2915, https://doi.org/10.1175/JAS-D-12-0340.1.

Yu, Z. H., 2002: The spiral rain bands of tropical cyclone and the vortex Rossby waves. *Acta Meteorologica Sinica*, **60**, 502–507, https://doi.org/10.3321/j.issn:0577-6619.2002.04.014. (in Chinese with English abstract)

Yue, C. J., S. T. Gao, L. Liu, and X. F. Li, 2015: A diagnostic study of the asymmetric distribution of rainfall during the landfall of typhoon Haitang (2005). *Adv. Atmos. Sci.*, **32**, 1419–1430, https://doi.org/10.1007/s00376-015-4246-0.

Zhang, X. Q., Z. Y. Ding, and Y. Wang, 2001: Actuality of high-jet and heavy rainfall caused by interaction between the mid-latitude synoptic system and typhoon. *Meteorological Monthly*, **27**, 3–8, https://doi.org/10.3969/j.issn.1000-0526.2001.08.001. (in Chinese with English abstract)

Zhao, S.-S., and X.-L. Wang, 2012: Decadal variations of extreme tropical cyclones influencing China during 1949-2009. *Advances in Climate Change Research*, **3**, 121–127, https://doi.org/10.3724/SP.J.1248.2012.00121.